

# On model based clustering of RNA-seq expression data

Kushal K Dey      Matthew Stephens

## Abstract

We propose a model based approach to cluster the reads level expression for bulk RNA and single cell RNA-seq data. It is similar to the topic model in Natural Language Processing and the admixture model in Population Genetics, that assigns grades of cluster membership to each sample. This approach provides us with easily interpretable cluster visualization and detects the underlying structure in the data better than distance based approaches. It also extracts the important genes that drive the clusters and provides measures of model fit to assess the strength of clustering. Further, we show that this method is robust under low coverage of reads. We apply this method on the GTEx tissue level bulk RNA expression data as well as two single cell RNA-seq data. Our methods are implemented in a R package **CountClust**, available at <https://github.com/kkdey/CountClust>.

## 1 Introduction

Clustering of samples based on gene expression data is a popular exploratory mechanism in bulk RNA-seq and single cell RNA-seq (scRNA-seq) experiments. It aids in quality control and helps in understanding the heterogeneity across tissue samples (bulk RNA-seq) or single cells (scRNA-seq). Usually the clustering techniques more commonly used in RNA-seq literature are distance based, primarily hierarchical and k-means clustering (see Jaitin *et al* 2014 [12], Buettner *et al* 2015 [18], GTEx Consortium paper [4]). However, the data obtained from the RNA sequencing experiments are counts data, representing the number of reads mapping to different genes. and there exist model based clustering methods based on counts which seem to be directly applicable to the RNA-seq reads data.

The clustering model we propose in this paper is similar to the topic model approach, widely used in Natural Language Processing (see Blei, Ng and Jordan 2003 [21], Blei and Lafferty 2009 [22]), which is derived from the Admixture model in population genetics (see Pritchard, Stephens and Donnelly 2000 [6]). This approach models each tissue sample as having some proportion of its reads coming from each cluster. This assumption is biologically sensible since in reality, each tissue sample indeed is a mixture of different cell types and presumably, the clusters under this model could be driven by the cell types. Also, such graded membership approach is capable of representing more continuous cluster patterns.

In this paper, we demonstrate that for RNA-seq (bulk or single cell) data with known structural patterns, such count clustering approach identifies the structure better than hierarchical clustering. It also allows one to interpret each cluster by providing information about genes

that are playing a significant role in driving the clusters and these genes may be important from both biological and medical standpoint. Also we show our method to be robust even for low coverage data as might be the case for single cell RNA-seq (scRNA-seq) data. We illustrate the performance of our method on GTEx tissue level bulk-RNA seq data as well as on two single cell data (due to Jaitin *et al* 2014 [12] and Zeisel *et al* 2015 [3]) .

## 2 Methods and Materials

### 2.1 Data preprocessing

We assume that the data from an RNA-seq experiment have been summarized by a table of counts  $C_{N \times G} = ((c_{ng}))$ , where  $c_{ng}$  is the number of RNA-seq reads from sample  $n$  that mapped to gene (or transcript)  $g$ . Such a table of counts is obtained by processing the BAM or FASTQ files obtained from sequencing machines and currently, there is an effort to make such reads table, ready for statistical analysis, publicly available (check the ReCounts website [2]). Before applying the graded membership model on the reads data, we remove the genes with 0 or same count of matched reads across all samples as they are non-informative for clustering. We also remove any sample or gene with NA values of reads and spike-in control genes, as the latter may create bias due to their typically having high number of reads mapped to them [1].

### 2.2 Model overview

The method we adopt allows each sample to have a grade of membership in the underlying clusters. This type of approach was first used in population genetics to model population samples as having parts of its genome derived from different clusters that represented ancestries (see Pritchard, Stephens and Donnelly 2000 [6]). Later, a similar approach was used to model documents to have grades of membership in different clusters, representing topics, depending on the frequencies of different words used (see Blei, Ng and Jordan 2003 [21]). In RNA-sequencing data too, each sample is viewed as having grades of membership in different underlying subpopulations (for e.g. cell types for tissue samples, cell phases for single cells etc).

We assume that the row vector of counts for each sample  $n$  across the genes follows a multinomial distribution.

$$c_{n*} \sim Mult(c_{n*}, p_{n*})$$

where  $c_{n*}$  is the count vector for the  $n$  th sample,  $c_{n*}$  is the sum of the counts in the vector  $c_{n*}$ , and  $p_{n*}$  is the probability that a read coming from sample  $n$  would get assigned to one of the  $G$  genes. The main idea is that this read could come from hidden subpopulations (may be cell types for tissue level expression study or cell cycle phases for single cell study) and its probability of getting assigned to some gene  $g$  may depend on which subpopulation it comes from. Denote the probability that the sample is coming from the  $k$  th subpopulation by  $q_{nk}$  ( $q_{nk} \geq 0$  and  $\sum_{k=1}^K q_{nk} = 1$  for each  $n$ ). Given that the sample is coming from the  $k$ th subgroup, the probability of a read being matched to the  $g$ th gene is given by  $\theta_{kg}$  ( $\theta_{kg} \geq 0$  and  $\sum_{g=1}^G \theta_{kg} = 1$  for  $k$ th subgroup). Then one can write

$$p_{ng} = \sum_{k=1}^K q_{nk} \theta_{kg} \quad \sum_{k=1}^K q_{nk} = 1 \quad \sum_{g=1}^G \theta_{kg} = 1$$

This model has  $N \times (K - 1) + K \times (G - 1)$  many unconstrained parameters, which is much smaller than the  $N \times G$  data values of counts. Usually for RNA-seq samples  $N$  varies in the region of 100s to 1000s and  $G$  ranges from 10,000 to 50,000 (depending on the underlying species and the types of genes tokenized) and  $K \ll \{N, G\}$ .

Due to the widespread use of topic models in Natural Language Processing literature, many softwares are available for fitting such models on document collections. Here, we use a Maximum a posteriori (MAP) estimation procedure implemented in R package **maptpx**(see Taddy 2012 [5]).

### 2.3 Visualization

A nice way to visualize the amount of relatedness among the samples is through the Structure plot, which is a popular tool to visualize the admixture patterns in population genetics based on SNP/ microsatellite data (see Rosenberg *et al* 2002 [7]). For each sample  $n$ ,  $q_{nk}$  represents the relative abundance of hidden subgroup  $k$  in the sample. The Structure plot assigns a color to each of the subgroups and then presents a vertical stacked barchart for each individual, with stack heights representing subgroup proportions and each subgroup assigned a particular color. If the colored patterns of two bars are similar, then the two samples must be closely related.

Another visualizing tool we recommend is t-distributed Stochastic Neighbor Embedding (t-SNE), which is well-suited for visualizing the high dimensional datasets on 2D, preserving the relative distance between samples in high dimension to a fair extent in 2D (see L.J.P. van der Maaten [10] and L.J.P. van der Maaten and Hinton [9]). t-SNE shows us which samples are close to each other when the data is projected on 2D. t-SNE is not a clustering tool and unlike Structure plot, does not show the relative abundance patterns of different subgroups in the sample. However, both Structure plot and t-SNE give a lot more interpretable visualization of the clustering compared to the heatmap and hierarchical clustering (see Results for illustration).

### 2.4 Cluster annotation

A question of considerable biological interest is which genes are significantly differentially expressed across the clusters, or in other words, which genes are driving the clustering. To answer this, we fix one cluster and for each gene, define a distance metric between that cluster and any of the other clusters, based on the cluster expression profile of the gene, namely the  $\theta$  values. For cluster  $k$ , we define the distance from cluster  $l$  based on expression profile of gene  $g$  to be

$$KL^g[k, l] := \theta_{kg} \log \frac{\theta_{kg}}{\theta_{lg}} + \theta_{lg} - \theta_{kg}$$

This is similar to the Kullback Leibler divergence of the Poisson distribution with parameter  $\theta_{lg}$  from another Poisson distribution with parameter  $\theta_{kg}$ . For each cluster  $k$ , we define the divergence measure for gene  $g$  as

$$Div^g[k] = \min_{l \neq k} KL^g[k, l]$$

The higher the divergence measure, the more significant is the role of the gene in the clustering. We choose a small subset of around 50-100 genes with highest values of  $Div^g[k]$  for each  $k$  and this set of genes can be viewed to be the most important genes driving the cluster  $k$ .

Once the most important driving genes for each cluster  $k$  have been extracted, we perform gene annotations on them using **mygene** R Bioconductor package (due to Mark A, Thompson R and Wu C 2014 [16]). We check if the driving genes for a particular cluster are associated with some specific biological functionality. This would validate whether the subgroups are biologically relevant.

### 3 Results

We begin by illustrating our method on the tissue level data from the GTEx project (V6 dbGaP accession phs000424.v6.p1, release date: Oct 19, 2015, <http://www.gtexportal.org/home/>) read counts data. RNA-seq data was obtained from 8555 samples collected from 450 donors across 51 tissues and 2 cell-lines. We collected a set of 16069 cis-genes that satisfied quality check (gene list available in [https://github.com/stephenslab/count-clustering/blob/master/utilities/gene\\_names\\_GTEX\\_V6.txt](https://github.com/stephenslab/count-clustering/blob/master/utilities/gene_names_GTEX_V6.txt)).

**Fig 1** presents the Structure plot for admixture model fit for  $K = 15$ . The Structure plot highlights the similarity among the samples coming from the same tissue and also tells us which tissues have similar patterns of gene expression. It is seen that the different Brain tissues seem to cluster together, the same being true for the arteries (Artery-aorta, Artery-tibial and Artery-coronary). Interestingly, Nerve Tibial and Adipose tissues (Adipose Subcutaneous and Adipose Visceral (Omentum)) also seem to have similar clustering patterns.

As observed from the Structure plot, some tissues seem to be assigned to separate clusters for  $K = 15$ , (e.g: Pancreas, Whole Blood), but other tissues are represented as an "admixed" version of multiple clusters (e.g: Thyroid). But in these latter cases, the samples coming from the same tissue all seem to be cluster together as they have very similar patterns of "admixing" of different clusters. A different way of visualizing the results, which highlights the clustering and separation of the different tissues on a 2D projection space (see **Supplementary Fig 1** [\[url\]](#)).

To biologically interpret the clusters in **Fig 1**, we performed cluster annotation (see Methods and Materials). **Tab ??** presents the gene IDs, names and a short summary of the functions of top 3 driving genes for each cluster. The cluster annotation in **Tab ??** highlights tissue specific

functions and pathways. We observe that *PRSS1* (protease serine 1), *CPA1* (carboxypeptidase) and *PNLIP* (pancreatic lipase) are the top three genes that drive the cluster separating Pancreas from the other tissues. Similarly, *HBB* (hemoglobin, beta), *HBA2* (hemoglobin, alpha 2) and *HBA1* (hemoglobin, alpha 1) seem to be the top three genes that distinguish Whole Blood and drive a separate cluster from the rest.

Although global analysis of all tissues is useful for highlighting major structure in the data, it is less well suited to identifying structure within tissues or among similar tissues. Therefore, we ran the analysis on samples from a particular tissue or similar tissues. **Fig 2** shows the Structure plot for  $K = 4$  on just the Brain samples. Brain Cerebellum and Cerebellar hemisphere seem to have 80 – 85% membership proportion in green cluster which seems distinctive. Recent stereological approaches have shown that rat cerebellum contains  $> 80\%$  neurons (Herculano-Houzel and Lent 2005) [15], much higher than other parts of the brain. We performed cluster annotation and observed that the pivotal genes that separated out the green cluster in brain cerebellum and cerebellar hemisphere are SNAP25 (synaptosomal-associated protein, 25kDa), ENO2 (enolase 2- gamma, neuronal) and CHGB (chromogranin B), all of which are associated with neuronal activities (see **Supplementary Table 1**). Therefore, the green cluster does seem to be driven by neuronal cell types, though not completely determined by them (since this cluster is almost non-existent in other parts of the Brain).

We aimed to assess the cluster performance of the graded membership method on lower coverage data as is observed in single cell RNA seq (scRNA seq) data. To compare the cluster performance between bulk-RNA coverage and single cell-RNA coverage, we thinned the GTEx reads data. If  $c_{ng}$  is the counts of number of reads mapping to gene  $g$  for sample  $n$  for the original data, then the thinned counts are given by

$$t_{ng} \sim \text{Bin}(c_{ng}, p_{thin})$$

where  $p_{thin}$  represents the proportional coverage of a single cell RNA-seq data compared to the bulk RNA-seq data. We compared the total library size between the GTEx tissue level data and the single cell data due to Jaitin *et al* [12] and observed that  $p_{thin} = 0.0001$ . We then used this thinning parameter and fitted the clustering model on  $t_{ng}$ s. **Fig 3** presents the Structure plot for  $K = 15$  for the thinned data. Many of the features from **Fig 1** are restored even after thinning, for instance the Brain tissues clustering together, Heart samples and Muscle Skeletal samples showing similar patterns. This implies that the clustering model is robust to the coverage of the data.

We next sought to demonstrate more quantitatively the utility of the model based clustering compared to other non model based clustering methods such as hierarchical clustering. In **Fig 4**, we consider every pair of tissues from the list of tissues in GTEx with number of samples  $> 50$ . Then we generated a set of 50 samples randomly drawn from the pooled set of samples coming from these two tissues and then observed whether the hierarchical and the admixture were separating out samples coming from the two different tissues. The same remains true for thinned GTEx data under different choices of thinning parameters. Check **Fig 6** for demon-

stration.

We applied the model on a couple of single cell datasets due to Jaitin *et al* [12] and Zeisel *et al* [3]. Jaitin *et al* sequenced around 4000 single cells from mouse spleen, where the cells were a heterogeneous mix enriched for expression of CD11c marker. The aim of their study was to separate out the B cells, NK cells, pDCs and monocytes. However the biological effect in their study was completely confounded with the amplification and sequencing batches. **Fig 5** (top panel) presents the Structure plot for  $K = 7$  for the Jaitin *et al* data with the samples arranged by their amplification batch (which was a refinement of the sequencing batch).

Zeisel *et al* analyzed the single cell data obtained from mouse cortex and hippocampus and obtained 47 molecularly distinct subclasses using marker genes, comprising all known major cell types in the region. **Fig 5** (bottom panel) presents the Structure plot for  $K = 10$  on their data, where the samples in Structure plot are grouped by their subclass assignment. It was interesting that the first few samples under Oligo6 seemed to show some membership from the red cluster, which was not observed in other Oligo6 samples. Within each group in the Structure plot, the samples are ordered in the same order as reported in the dataset and so, there is a possibility that these peculiarities in Oligo6 samples may result from the fact that either these first few Oligo6 samples were misclassified by the algorithm the authors used (some Oligo4 samples show similar patterns to these samples) or the difference may result from these samples being sequenced in a plate or in a sequencing lane different from the rest of the Oligo6 samples.

**Fig 5** highlights the need for caution regarding interpreting Admixture results or any clustering results, as there is a possibility of technical effects driving the clusters instead of true biological effects. There has been a growing concern among biostatisticians today about how to deal with batch effects [13] [14].

## 4 Discussions

We have presented a model based clustering approach for RNA-seq (bulk or single cell) read counts data which models each sample as having a mixed membership in different clusters and also helps identifying genes driving the clusters, which may be of significant bio-medical importance. Our approach is an alternative to the distance based methods of clustering, for instance hierarchical clustering, and it seems to outperform the latter in separating biologically meaningful groups in our tests.

Deconvolution techniques using marker genes are popularly used to learn about the the concentration of different cell types in a cell mixture and cell type signature expression profiles. Our technique is analogous to blind deconvolution approach which estimates the cell type proportions and cell type signatures jointly (see Schwartz *et al* 2010 [26] and Repsilber *et al* 2010 [25]), except that we operate under Poisson model framework to model the counts data. This fully unsupervised approach, however, seems to fail in identifying clusters determined completely by individual cell types. Proposed alternatives to blind deconvolution approach include

two-pronged sequential updating of the cell type concentration and cell type proportion (see Lindsay *et al* [27]) and supervised or semi-supervised learning where it is assumed that some information of cell type signature expression profiles is known (see Shen-Orr *et al* 2010 [?], Qiao *et al* 2012 [24]). As part of our future works, we plan to implement similar modifications to our method so as to make the clusters more biologically interpretable.

Since our method is model based, it provides an optimal  $K$  for the model fit. However, one has to run the model on the data for a range of  $K$ 's and that is not always practical when running the model on large datasets as in RNA-seq reads data. For a single run with the algorithm running till the successive log posterior increase is less than 0.01, the computation time for the algorithm was approximately 33.4 mins for Jaitin *et al* [12] single cell experiment ( $K = 7$ ), 59.8 mins for Zeisel *et al* single cell experiment ( $K = 10$ ) and 3297.4 mins for GTEx V6 data ( $K = 15$ ).

So far, in our studies, we fitted the model on the entire RNA-seq reads data, comprising of all the genes. In reality, most of the genes will not be informative about the clusters and an efficient variable selection algorithm, if incorporated with the clustering algorithm, can lead to significant speed up without much loss of information. This is a future direction to this work we are interested in. Another point of biological interest would be to perform cluster annotation of genetic pathways which would be more meaningful as genes often act together with other genes in pathways related to different activities.

The methods discussed in this paper are implemented in the package **CountClust** available on Github (<https://github.com/kkdey/CountClust>) which is a wrapper package of **maptpx** due to Matt Taddy [5].

## References

1. Jiang L, Schlesinger F, Davis CA, Zhang Y, Li R, Salit M, Gingeras TR and Oliver B. *Synthetic spike-in standards for RNA-seq experiments*. Genome Res, 2011;21, 1543-1551
2. Frazee AC, Langmead B, Leek JT. *ReCount: a multi-experiment resource of analysis-ready RNA-seq gene count datasets*. BMC Bioinformatics, 2011, 12:449.
3. Amit Zeisel, Ana B. Muoz-Manchado, Simone Codeluppi, Peter Linnerberg, Gioele La Manno, Anna Jurus, Sueli Marques, Hermany Munguba, Liqun He, Christer Betsholtz, Charlotte Rolny, Gonalo Castelo-Branco, Jens Hjerling-Leffler, and Sten Linnarsson. *Cell types in the mouse cortex and hippocampus revealed by single-cell RNA-seq*. Science 6 March 2015: 347 (6226), 1138-1142.
4. The GTEx Consortium. *The Genotype-Tissue Expression (GTEx) project*. Nature genetics. 2013;45(6):580-585. doi:10.1038/ng.2653.
5. Matt Taddy. *On Estimation and Selection for Topic Models*. AISTATS 2012, JMLR W&CP 22. (maptpx R package).

6. Pritchard, Jonathan K., Matthew Stephens, and Peter Donnelly. *Inference of population structure using multilocus genotype data*. Genetics 155.2 (2000): 945-959.
7. Rosenberg NA, Pritchard JK, Weber JL, Cann HM, Kidd KK, Zhivotovsky LA and Feldman MW. The genetic structure of human populations. Science 2002, 298: 2381-2385.
8. Anil Raj, Matthew Stephens, and Jonathan K. Pritchard. *fastSTRUCTURE: Variational Inference of Population Structure in Large SNP Data Sets*. Genetics.2014 197:573-589.
9. L.J.P. van der Maaten and G.E. Hinton. *Visualizing High-Dimensional Data Using t-SNE*. Journal of Machine Learning Research, 2008: 2579-2605.
10. L.J.P. van der Maaten. *Accelerating t-SNE using Tree-Based Algorithms*. Journal of Machine Learning Research, 2014:3221-3245.
11. Mark A, Thompson R and Wu C. *mygene: Access MyGene.Info services*. 2014. R package version 1.2.3.
12. Jaitin DA, Kenigsberg E et al. *Massively Parallel Single-Cell RNA-Seq for Marker-Free Decomposition of Tissues into Cell Types*. Science, 2014: 343 (6172) 776-779.
13. Jeffrey T. Leek, Robert B. Scharpf, Hector C Bravo, David Simcha, Benjamin Langmead, W. Evan Johnson, Donald Geman, Keith Baggerly and Rafael A. Irizarry *Tackling the widespread and critical impact of batch effects in high-throughput data*. Nature Reviews Genetics 11, 733-739.
14. Stephanie C Hicks, Mingxiang Teng and Rafael A Irizarry *On the widespread and critical impact of systematic bias and batch effects in single-cell RNA-Seq data*. BiorXiv, <http://biorxiv.org/content/early/2015/09/04/025528>
15. Herculano-Houzel S and Lent R. *Isotropic fractionator: a simple, rapid method for the quantification of total cell and neuron numbers in the brain*. J Neurosci. 2005 Mar 9;25(10), 2518-21.
16. Mark A, Thompson R and Wu C. *mygene: Access MyGene.Info services. R package version 1.2.3*.
17. Grn D, Lyubimova A, Kester L, Wiebrands K, Basak O, Sasaki N, Clevers H, van Oudenaarden A. *Single-cell messenger RNA sequencing reveals rare intestinal cell types*. Nature. 2015 Sep 10;525(7568), 251-5.
18. Buettner F, Natarajan KN, Casale FP, Proserpio V, Scialdone A, Theis FJ, Teichmann SA, Marioni JC and Stegle O. *Computational analysis of cell-to-cell heterogeneity in single-cell RNA-sequencing data reveals hidden subpopulations of cells* Nature Biotechnology 2015, 33, 155-160, doi:10.1038/nbt.3102
19. Palmer C, Diehn M, Alizadeh AA and Brown PO. *Cell-type specific gene expression profiles of leukocytes in human peripheral blood*. BMC Genomics 2006, 7:115.



20. Flutre T, Wen X, Pritchard J and Stephens M. *A Statistical Framework for Joint eQTL Analysis in Multiple Tissues* PLoS Genet 2013, 9(5): e1003486. doi:10.1371/journal.pgen.1003486
21. Blei DM, Ng AY and Jordan MI. *Latent Dirichlet Allocation* Journal of Machine Learning Research 2003, 3, 993-1022
22. Blei DM and Lafferty J. *Topic Models* In A. Srivastava and M. Sahami, editors, Text Mining: Classification, Clustering, and Applications . Chapman & Hall/CRC Data Mining and Knowledge Discovery Series, 2009.
23. Shen-Orr SS, Tibshirani R, Khatri, P, Bodian DL, Staedtler F, Perry NM, Hastie, T, Sarwal MM, Davis MM, Butte AJ. Cell typespecific gene expression differences in complex tissues. Nature Methods 2010, 7(4), 287-289
24. Qiao W, Quon G, Csaszar E, Yu M, Morris Q, Zandstra PW PERT: A Method for Expression Deconvolution of Human Blood Samples from Varied Microenvironmental and Developmental Conditions. PLoS Comput Biol 2012, 8(12)
25. Repsilber D, Kern S, Telaar A, Walzl G, Black GF, Selbig J, Parida SK, Kaufmann SH, Jacobsen M. Biomarker discovery in heterogeneous tissue samples -taking the in-silico deconfounding approach. BMC bioinformatics 2010, 11(1), 27+
26. Schwartz R, Shackney SE. Applying unmixing to gene expression data for tumor phylogeny inference. BMC bioinformatics 2010, 11(1), 42+
27. Lindsay J, Mandoiu I, Nelson C. Gene Expression Deconvolution using Single-cells <http://dna.engr.uconn.edu/bibtexmgr/upload/Lal.13.pdf>.

**Figure 1.** Structure plot of the admixture proportions (with 15 topics/clusters) for the 8555 tissue samples coming from 53 tissues in GTEx V6 data based on 16069 cis genes derived using PEER analysis MatrixEQTL . Note that the samples coming from the same tissue have similar admixing patterns. Tissues of same origin, for instance all the brain tissues, all the arteries seem to cluster together. Also, some other tissues, presumably not of same origin, show markedly similar clustering patterns - for instance Breast mammary tissue, Nerve Tibial and Adipose tissues are very similar in clustering patterns.

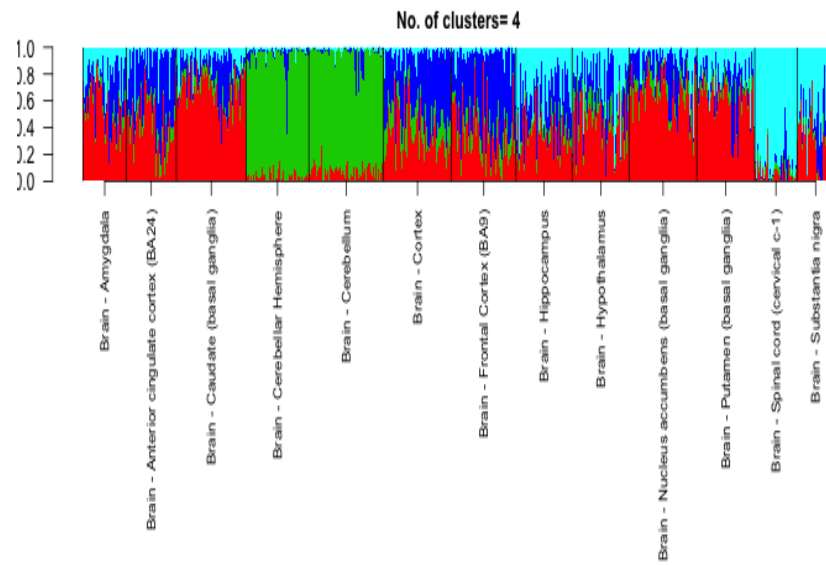


**Figure 2.** Structure plot of the admixture proportions (with 4 clusters) for the brain tissue samples drawn from GTEx Version 4 data. Quite clearly, brain cerebellum and cerebellar hemisphere seem to be dominated by the blue cluster while the Spinal cord and Substantia nigra by the cyan cluster. Prior marker based approaches have verified that  $> 80\%$  of cells in brain cerebellum correspond to neurons [15]. So, the blue cluster seems to be driven by the neuron cell type. This fact is further attested by the gene annotations of the top genes driving the blue cluster (Supplementary Table 1).

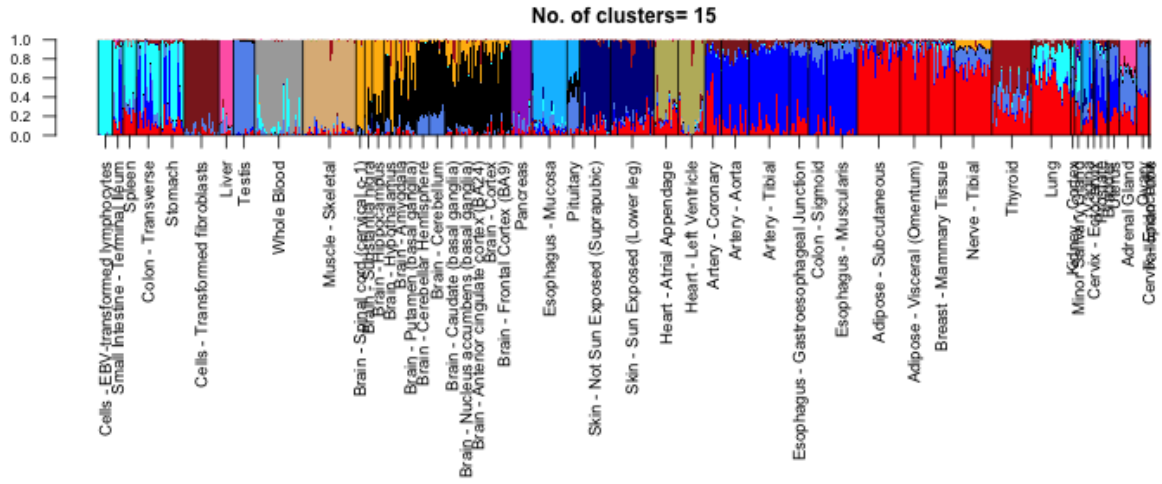
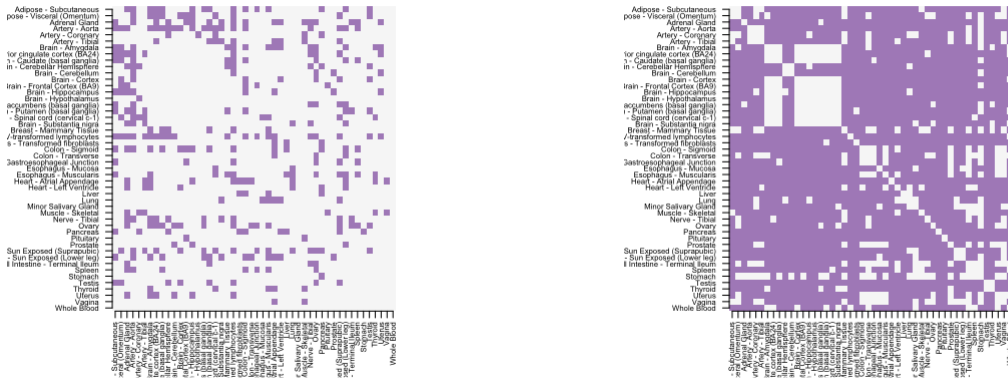


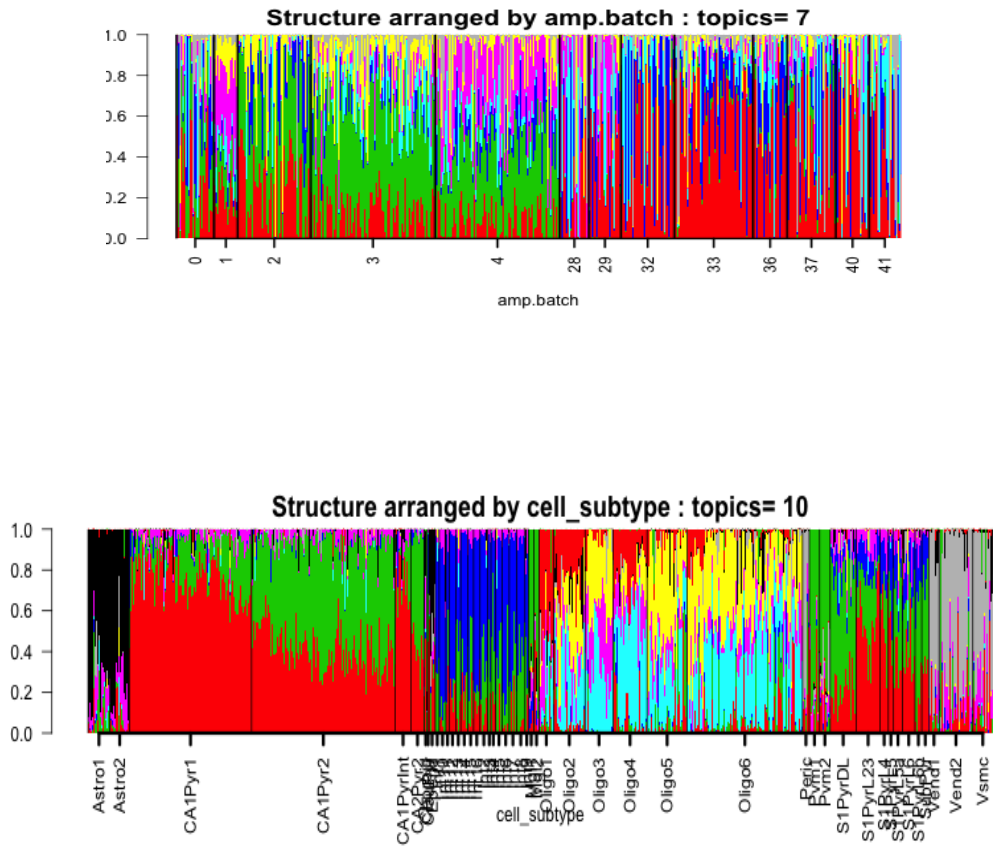
**Figure 3.** Structure plot of all tissue samples in GTEx V6 data thinned data with  $p_{thin} = 0.0001$  for  $K = 15$ . The thinning parameter has been chosen so that the GTEx RNA-seq data can be interpreted at the same scale as a scRNA-seq data. The clustering patterns are more noisy compared to the non-thinned data in Fig 1, but overall, the similarity patterns across the tissues are retained. For instance, the brain tissues and the arteries still seem to be clustering together.



(a) hierarchy thin 0.1

(b) admixture thin 0.1

**Figure 4.** A comparison of the hierarchical method with the admixture method. For each pair of tissues, we selected randomly 50 samples and then on the reads data for these 50 samples, we applied the hierarchical clustering method with complete linkage and Euclidean distance and then cut the tree at  $K = 2$ . We then observed if it separates out the samples coming from the two tissues, in case it does, we color the cell corresponding to that pair of tissues. We apply admixture model on the same data for  $K = 2$ . Then we fixed one cluster, observed the proportions for that cluster, sorted the samples based on the proportions for that cluster and separated out the samples at the point of maximum jump/fall in the proportions for that cluster. If that separates out the two tissues, we color the cell, else keep it blank. From the graph it seems that the admixture model has been far more successful in separating out different tissues compared to the hierarchical method.



(a)  $k = 10$

**Figure 5.** (*top panel*) Structure plot of the 1041 single cells for  $K=7$  of the Jaitin *et al* data [12] arranged by the amplification batch. It is observed that the clustering patterns within each batch are similar and so, either the amplification batch is driving the clustering or it is confounded with the actual biological effects, making it difficult to interpret these clusters. (*bottom panel*) Structure plot of all samples for  $K = 10$  of Zeisel *et al* data [3], arranged by the cell subtype labels that were determined by the authors using their BackSpin algorithm and subsequent marker gene annotations. While the cluster patterns within these cell subtypes are similar in general, the first few samples in Oligo6 show mild presence of red cluster and are markedly different from the rest of the samples in Oligo6 which do not show any trace of red cluster. These first few samples of Oligo6 look similar in pattern to some Oligo4 samples with mild red cluster presence. Oligo4 samples also shows some heterogeneity in terms of the proportion of red cluster present. This could either be due to misclassification of the Backspin algorithm, or due to technical effects unaccounted for (like plate effect, lane effect etc).

## 4.1 Supplemental figures

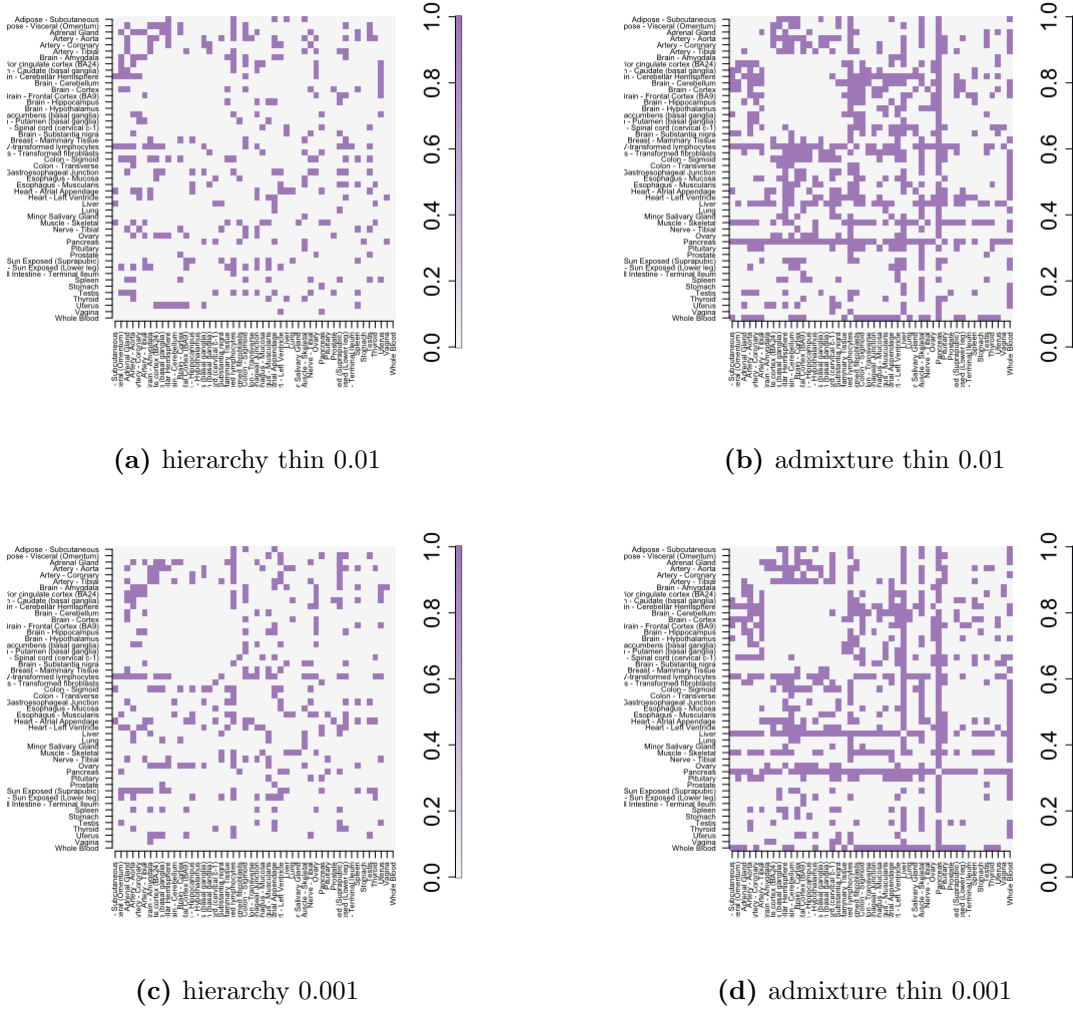


**Figure 6.** In this graph, we compare the hierarchical clustering method with the admixture method for thinned data with thinning parameters being  $p_{thin} = 0.001$  and  $p_{thin} = 0.0001$ . The color coding scheme is similar to **Fig 4**. Note that the performance of the admixture indeed deteriorates from **Fig 4** in separating out the clusters as is expected. But it still outperforms the hierarchical clustering.



Cluster	Gene names	Proteins	Summary
cluster red (Nerve, Adipose)	ENSG00000170323	fatty acid binding protein 4, adipocyte	FABP4 encodes the fatty acid binding protein found in adipocytes, roles include fatty acid uptake, transport, and metabolism
	ENSG00000189058	apolipoprotein D	encodes a component of high density lipoprotein that has no marked similarity to other apolipoprotein sequences, closely associated with lipoprotein metabolism.
	ENSG00000166819	perilipin 1	coats lipid storage droplets in adipocytes, thereby protecting them until they can be broken down by hormone-sensitive lipase.
cluster blue (Ar- teries, Esophagus)	ENSG00000133392	myosin, heavy chain 11, smooth muscle	functions as a major contractile protein, converting chemical energy into mechanical energy through the hydrolysis of ATP.
	ENSG00000107796	actin, alpha 2, smooth muscle, aorta	protein encoded by this gene belongs to the actin family of proteins, which are highly conserved proteins that play a role in cell motility, structure and integrity, defects in this gene cause aortic aneurysm familial thoracic type 6.
	ENSG00000163017	actin, gamma 2, smooth muscle, enteric	encodes actin gamma 2; a smooth muscle actin found in enteric tissues, involved in various types of cell motility and in the maintenance of the cytoskeleton.
cluster shallow blue (Brain)	ENSG00000197971	myelin basic protein	major constituent of the myelin sheath of oligodendrocytes and Schwann cells in the nervous system
	ENSG00000131095	glial fibrillary acidic protein	encodes one of the major intermediate filament proteins of mature astrocytes, mutations causes Alexander disease.
	ENSG00000132639	synaptosomal-associated protein, 25kDa	this gene product is a presynaptic plasma membrane protein involved in the regulation of neurotransmitter release.

Cluster	Gene names	Proteins	Summary
cluster black (Testis)	ENSG00000122304	protamine 2	<p>Protamines are the major DNA-binding proteins in the nucleus of sperm</p> <p>Protamines are the major DNA-binding proteins in the nucleus of sperm</p> <p>This gene is expressed in the testis in Sertoli cells but not germ cells, regulates spermatogenesis.</p>
	ENSG00000175646	protamine 1	
	ENSG00000010318	PHD finger protein 7	
cluster light blue (Thy- roid, Stomach)	ENSG00000042832	thyroglobulin	<p>thyroglobulin produced predominantly in thyroid gland, synthesizes thyroxine and triiodothyronine, associated with Graves disease and Hashimoto thyroiditis.</p> <p>encodes gastric lipase, an enzyme involved in the digestion of dietary triglycerides in the gastrointestinal tract, and responsible for 30 % of fat digestion processes occurring in human.</p> <p>encodes an aspartic proteinase that belongs to the peptidase family A1. The encoded protein is a digestive enzyme that is produced in the stomach and constitutes a major component of the gastric mucosa, associated with susceptibility to gastric cancers.</p>
	ENSG00000182333	lipase, gastric	
	ENSG00000096088	progastricsin (pepsinogen C)	
cluster deep blue (Skin)	ENSG00000186395	keratin 10, type I	<p>encodes a member of the type I (acidic) cytokeratin family, mutations associated with epidermolytic hyperkeratosis.</p> <p>specifically expressed in the spinous and granular layers of the epidermis with family member KRT10 and mutations in these genes have been associated with bullous congenital ichthyosiform erythroderma.</p> <p>expressed largely in the upper spinous layer of epidermal keratinocytes and mutations in this gene have been associated with bullous congenital ichthyosiform erythroderma.</p>
	ENSG00000167768	keratin 1, type II	
	ENSG00000172867	keratin 2, type II	
cluster dark brown (Cells fibroblasts)	ENSG00000115414	fibronectin 1	<p>Fibronectin is involved in cell adhesion, embryogenesis, blood coagulation, host defense, and metastasis.</p> <p>Mutations in this gene associated with osteogenesis imperfecta types I-IV, Ehlers-Danlos syndrome type and Classical type, Caffey Disease.</p> <p>Mutations in this gene associated with osteogenesis imperfecta types I-IV, Ehlers-Danlos syndrome type and Classical type, Caffey Disease.</p>
	ENSG00000108821	collagen, type I, alpha 1	
	ENSG00000164692	collagen, type I, alpha 2	

Cluster	Gene names	Proteins	Summary
cluster shallow yellow (Lung)	ENSG00000168878	surfactant protein B	an amphipathic surfactant protein essential for lung function and homeostasis after birth, mutations cause pulmonary alveolar proteinosis, fatal respiratory distress in the neonatal period.
	ENSG00000185303	surfactant protein A2	Mutations in this gene and a highly similar gene located nearby, which affect the highly conserved carbohydrate recognition domain, are associated with idiopathic pulmonary fibrosis.
	ENSG00000122852	surfactant protein A1	encodes a lung surfactant protein that is a member of a subfamily of C-type lectins called collectins, associated with idiopathic pulmonary fibrosis.
cluster yellow (Muscle skeletal)	ENSG00000109061	myosin, heavy chain 1, skeletal muscle, adult	a major contractile protein which converts chemical energy into mechanical energy through the hydrolysis of ATP.
	ENSG00000183091	nebulin	encodes nebulin, a giant protein component of the cytoskeletal matrix that coexists with the thick and thin filaments within the sarcomeres of skeletal muscle, associated with recessive nemaline myopathy.
	ENSG00000125414	myosin, heavy chain 2, skeletal muscle, adult	encodes a member of the class II or conventional myosin heavy chains, and functions in skeletal muscle contraction.
cluster grey (Whole Blood)	ENSG00000244734	hemoglobin, beta	mutant beta globin causes sickle cell anemia, absence of beta chain/ reduction in beta globin leads to thalassemia.
	ENSG00000188536	hemoglobin, alpha 2	deletion of alpha genes may lead to alpha thalassemia.
	ENSG00000206172	hemoglobin, alpha 1	deletion of alpha genes may lead to alpha thalassemia.
cluster cyan (Heart)	ENSG00000175206	natriuretic peptide A	protein encoded by this gene belongs to the natriuretic peptide family, associated with atrial fibrillation familial type 6.
	ENSG00000197616	myosin, heavy chain 6, cardiac muscle, alpha	encodes the alpha heavy chain subunit of cardiac myosin, mutations in this gene cause familial hypertrophic cardiomyopathy and atrial septal defect 3.
	ENSG00000159251	actin, alpha, cardiac muscle 1	protein encoded by this gene belongs to the actin family, associated with idiopathic dilated cardiomyopathy (IDC) and familial hypertrophic cardiomyopathy (FHC).

Cluster	Gene names	Proteins	Summary
cluster shallow green (Esophagus mucosa)	ENSG00000171401	keratin 13, type I	protein encoded by this gene is a member of the keratin gene family, associated with the autosomal dominant disorder White Sponge Nevus.
	ENSG00000170477	keratin 4, type II	protein encoded by this gene is a member of the keratin gene family, associated with White Sponge Nevus, characterized by oral, esophageal, and anal leukoplakia.
	ENSG00000143536	cornulin	may play a role in the mucosal/epithelial immune response and epidermal differentiation.
cluster light brown (Pancreas)	ENSG00000204983	protease, serine 1	secreted by pancreas, associated with pancreatitis
	ENSG00000091704	carboxypeptidase A1	secreted by pancreas, linked to pancreatitis and pancreatic cancer
	ENSG00000175535	pancreatic lipase	encodes a carboxyl esterase that hydrolyzes insoluble, emulsified triglycerides, and is essential for the efficient digestion of dietary fats. This gene is expressed specifically in the pancreas.
cluster violet (Liver)	ENSG00000171195	mucin 7, secreted	encodes a small salivary mucin, which is thought to play a role in facilitating the clearance of bacteria in the oral cavity and to aid in mastication, speech, and swallowing, associated with susceptibility to asthma.
	ENSG00000163631	albumin	functions primarily as a carrier protein for steroids, fatty acids, and thyroid hormones and plays a role in stabilizing extracellular fluid volume.
	ENSG00000257017	haptoglobin	encodes a preproprotein, which is processed to yield both alpha and beta chains, which subsequently combine as a tetramer to produce haptoglobin, linked to diabetic nephropathy, Crohn's disease, inflammatory disease behavior, primary sclerosing cholangitis and reduced incidence of Plasmodium falciparum malaria.
cluster salmon (Pituitary)	ENSG00000172179	prolactin 2	encodes the anterior pituitary hormone prolactin. This secreted hormone is a growth regulator for many tissues, including cells of the immune system.
	ENSG00000259384	growth hormone 1	expressed in the pituitary, play an important role in growth control, mutations in or deletions of the gene lead to growth hormone deficiency and short stature.
	ENSG00000115138	proopiomelanocortin	synthesized mainly in corticotroph cells of the anterior pituitary, mutations in this gene have been associated with early onset obesity, adrenal insufficiency, and red hair pigmentation.

## 4.2 Supplementary Table 1

Cluster	Gene names	Proteins	Summary
cluster 1, red	ENSG00000018625	ATPase, Na <sup>+</sup> /K <sup>+</sup> transporting, alpha 2 polypeptide	responsible for establishing and maintaining the electrochemical gradients of Na and K ions across the plasma membrane, mutations in this gene result in familial basilar or hemiplegic migraines, and in a rare syndrome known as alternating hemiplegia of childhood.
	ENSG00000120885	clusterin	protein encoded by this gene is a secreted chaperone that can under some stress conditions also be found in the cell cytosol, also involved in cell death, tumor progression, and neurodegenerative disorders.
	ENSG00000132002	DnaJ (Hsp40) homolog, subfamily B, member 1	encodes a member of the DnaJ or Hsp40 (heat shock protein 40 kD) family of proteins, that stimulates the ATPase activity of Hsp70 heat-shock proteins to promote protein folding and prevent misfolded protein aggregation.
cluster 2, green	ENSG00000132639	synaptosomal-associated protein, 25kDa	Synaptic vesicle membrane docking and fusion is mediated by SNAREs located on the vesicle membrane (v-SNAREs) and the target membrane (t-SNAREs), involved in the regulation of neurotransmitter release.
	ENSG00000111674	enolase 2 (gamma, neuronal)	encodes one of the three enolase isoenzymes found in mammals, is found in mature neurons and cells of neuronal origin.
	ENSG00000089199	chromogranin B	encodes a tyrosine-sulfated secretory protein abundant in peptidergic endocrine cells and neurons. This protein may serve as a precursor for regulatory peptides.
cluster 3, blue	ENSG00000160014	calmodulin 3 (phosphorylase kinase, delta)	is a calcium binding protein that plays a role in signaling pathways, cell cycle progression and proliferation.
	ENSG00000127585	F-box and leucine-rich repeat protein 16	Members of the F-box protein family, such as FBXL16, are characterized by an approximately 40-amino acid F-box motif.
	ENSG00000154277	ubiquitin carboxyl-terminal esterase L1	specifically expressed in the neurons and in cells of the diffuse neuroendocrine system. Mutations in this gene may be associated with Parkinson disease.
cluster 4, cyan	ENSG00000197971	myelin basic protein	protein encoded is a major constituent of the myelin sheath of oligodendrocytes and Schwann cells in the nervous system.
	ENSG00000133392	glial fibrillary acidic protein	encodes major intermediate filament proteins of mature astrocytes, a marker to distinguish astrocytes during development, mutations in this gene cause Alexander disease, a rare disorder of astrocytes in central nervous system.
	ENSG00000107796	secreted protein, acidic, cysteine-rich (osteonectin)	encodes a cysteine-rich acidic matrix-associated protein, required for the collagen in bone to become calcified, in extracellular matrix synthesis and cell shape promotion, associated with tumor suppression.